

Density of states and group velocity of electrons in SiO₂ calculated from a full band structure

Elena Gnani, Susanna Reggiani, and Massimo Rudan

*Advanced Research Center for Electronics Systems—Dipartimento di Elettronica, Informatica e Sistemistica,
University of Bologna, Viale Risorgimento 2, 40136 Bologna, Italy*

(Received 14 May 2002; revised manuscript received 22 August 2002; published 11 November 2002)

The full band structure of SiO₂ has been determined in order to calculate parameters that are necessary for the description of carrier transport. *Ab initio* calculations of the density of states and group velocity for the conduction bands of SiO₂ are worked out as a function of energy. Four different crystal structures of SiO₂ are investigated, which are known to be built up by the same fundamental unit, namely, the SiO₄ tetrahedron: they are the α - and β -quartz and the α - and β -cristobalite. All of them are polymorphs of silica. The conduction bands are calculated by means of two different techniques: the Hartree-Fock method and density-functional theory. The different features of the two methods are examined. Eight energy bands are used to calculate the density of states and group velocity for the energies of interest. Based on such calculations, the relevant scattering mechanisms have been modeled to determine the microscopic relaxation times. This in turn allows for the solution of the Boltzmann transport equation in the coordinate and energy space, which eventually leads to the calculation of macroscopic quantities such as carrier concentration, average velocity, and average energy. Examples are given of calculated electron mobility and average energy, along with comparisons with experimental results available in the literature.

DOI: 10.1103/PhysRevB.66.195205

PACS number(s): 71.20.-b, 72.10.-d, 71.15.-m, 72.20.-i

I. INTRODUCTION

Among insulators, silicon dioxide plays a major role in the solid-state technology. Especially in recent years, experimental and theoretical investigations focused on microscopic properties of this material related with reliability problems. The hot-carrier effects and, among them, those related to carrier injection into the gate oxide, cannot be neglected any more in ultrascaled devices. A first-order model of electron transport in silicon dioxide has already been worked out in the framework of the spherical-harmonics expansion (SHE) method applied to the solution of the Boltzmann transport equation.¹ One of the main advantages of this method is that it provides the carrier-distribution function in the physical space and energy in a deterministic way. Thus, the information about the carriers' energy distribution is maintained, which is essential for describing high-energy phenomena. In Ref. 1, the scattering rates for each collision process have been analyzed and a number of transport properties of electrons in bulk SiO₂ have been worked out in the framework of the parabolic-band approximation. Moreover, a new model has been introduced into the SHE code to calculate the microscopic fluxes at the silicon interface.² The description of the high-energy tail of the distribution function above the energy barrier at the interface and within SiO₂ provides useful information about the electron injection into the gate oxide.

As far as the investigation of carrier transport in SiO₂ is concerned, the main theoretical efforts were via Monte Carlo simulation.³⁻⁵ In these works microscopic collision mechanisms in polar materials have accurately been modeled, leading to interpretation of the experimental data for average velocity, average energy, and impact ionization in SiO₂. In our first investigation¹ of the electron transport in SiO₂ some approximations were embedded in the description of the band structure at higher energies. In particular, the first con-

duction band was assumed to be a spherical and parabolic function terminating at 6 eV, this limiting the validity of the analysis when high electric fields are considered.

A more accurate description of the transport properties at higher energies, suitable for the application of the SHE method, requires two steps: (i) the calculation of the full band structure over the first Brillouin zone, and (ii) the consistent calculation—from the full band structure—of the fundamental functions that are necessary in the SHE method, namely, the density of states and group velocity as a function of energy. The work presented in this paper illustrates the outcome of such calculations in SiO₂. The paper extends the results of Ref. 6, where the solution of the Schrödinger equation (namely, step *i* above) was carried out along specific crystalline directions only. As in Ref. 6, two different *ab initio* techniques [Hartree-Fock (HF) and density-functional theory (DFT)] are adopted here. In particular, the gradient-corrected extension⁷ of the local-density approximation (LDA) has been used in the DFT technique. The nonhomogeneous electron-gas effects have been accounted for through the Lee-Yang-Parr functional.⁸

As in the SHE scheme the band structure of the material appears through the density of states and group velocity, the calculations reported in this work constitute the basis to achieve an accurate description of the transport properties for SiO₂ at higher energies. Obviously, the completion of a research project aiming at modeling the carrier transport requires the description of the collision events; in particular, as far as SiO₂ is concerned, the implementation of the electron-phonon interactions has already occurred in Ref. 1 for the spherical-parabolic approximation of the band structure. Owing to the calculation of the transport parameters presented in this paper, the investigation on the collision events has been extended to the high-energy case, and the results are reported at the end of the paper.

The description of some electronic properties of the SiO₂

polymorphs has been addressed as early as the late 1970's in Refs. 9–12. The tight-binding technique has been applied in Refs. 9 and 11, which report the calculation of the conduction bands of the ideal β -cristobalite at the three high-symmetry points of the \mathbf{k} space and estimate the effective mass of the lowest conduction band. A similar calculation is shown in Ref. 12 for α -quartz. In Ref. 10 the pseudopotential technique is applied to α -quartz to determine the eigenvalues in 16 points of the irreducible Brillouin zone and to calculate the effective mass of electrons and holes. A self-consistent LDA approach was later used in Ref. 13 to calculate the conduction and valence bands of SiO_2 polymorphs. The LDA technique adopted in Ref. 13 is based on the assumption of a locally homogeneous electron gas. Among the aims of the present work are overcoming some of the approximations of the investigations mentioned above, and consistently extending the calculation in order to determine the density of states and group velocity. References exist where the density of states is calculated for materials different from SiO_2 , e.g., hexagonal SiC polytypes,¹⁴ band-tail derivation in semiconductors,¹⁵ and bulk and interface density of states in amorphous- or polycrystalline-silicon devices.¹⁶ In recent papers, calculations have been reported for ultrathin SiO_2 : tight-binding and *ab initio* calculations have been used in Refs. 17 and 18, respectively, in the framework of investigations on the applicability of the effective-mass approximation to the carrier dynamics, including tunneling. On the other hand, to our knowledge the calculation of the group velocity in SiO_2 polymorphs has not been tackled before.

The paper is organized as follows: in Sec. II, the electronic properties of SiO_2 are analyzed and the choice of the SiO_2 polymorphs is discussed. The description of the physical model for the electrons in SiO_2 is briefly illustrated in Sec. III. In Sec. IV the first Brillouin zone of the crystalline systems is described along with the numerical details about the three-dimensional mesh adopted in the \mathbf{k} space. The computational details for the calculation of the density of states and group velocity are given in Sec. V. The optimization of the basis sets adopted for the polymorphs of SiO_2 is described in Sec. VI. Finally, the results are shown in Sec. VII. They consist of the density of states and group velocity of the polymorphs considered, in the calculations of the electron mobility and average energy, and in the comparison with experimental data available in the literature.

II. THE POLYMORPHS OF SiO_2

In very-large-scale integrated complementary metal-oxide semiconductor (CMOS) technology, the gate oxide is grown in an amorphous phase on a silicon crystal: this means that SiO_2 is constituted by SiO_4 tetrahedra with bond-length and bond-angle distortions. It is known that most amorphous phases are characterized by distortions of about 1% for the bond length and 10% for the bond angle, thus the main difference between the crystalline and amorphous phases is due to the Si–O–Si bonding.¹⁹ Moreover, it has experimentally been observed that the x-ray photoemission spectra²⁰ and ultraviolet photoemission spectra²¹ of amorphous and crystalline SiO_2 appear to be quite similar in the location and

global shape of the peaks. As a consequence, the calculation of the electronic properties of the crystalline phases of SiO_2 can be exploited to understand the main aspects of the amorphous phases as well.

The set of polymorphs that have been analyzed in this work has been selected with the aim of taking into account forms with an electronic density similar to that of the amorphous silicon dioxide, and with a quite symmetric crystalline structure.⁶ Among the SiO_2 polymorphs, the α -quartz form of silica is the most common structure present in nature and has 6 symmetry operators. The β -quartz structure is similar to that of α -quartz, but is characterized by 12 symmetry operators, this providing a computational advantage in terms of central processing unit time and memory in the calculation of a number of physical properties. The α -cristobalite structure is characterized by 8 symmetry operators, but its structure is less compact in comparison with that of quartz. The β -cristobalite is characterized by a diamond structure with an oxygen atom placed on each vertex of the cell, and, due to its 48 symmetry operators, it can be seen as the most suitable form for *ab initio* calculations.

The numerical calculation of the band structure and density of states implies the solution of a many-body problem that exceeds the computational power of nowadays computers. From the theoretical standpoint, such calculations can be dealt with by methods similar to those used for analyzing molecular structures. In that field, a number of theories have been developed for the purpose of simulating molecular structures that are known to reduce the complexity of the simulation by means of suitable approximations. Among these are the HF method and DFT, which are implemented in the code CRYSTAL98© adopted in this work to analyze the crystalline forms under investigation.²² Both approaches have suitably been extended in Ref. 22 to solve the one-electron Schrödinger equation for the periodical problem of a crystalline structure.

III. COEFFICIENTS OF THE TRANSPORT MODEL

One of the main properties of the spherical-harmonics expansion method is that it provides the carriers' energy distribution in the real space-energy domain (\mathbf{r}, E) in a deterministic way.²³ This feature is obtained by expanding the carrier-distribution function $f(\mathbf{r}, \mathbf{k})$ in the momentum space in series of spherical harmonics defined on the unit sphere.^{24–26} The method eventually yields a system of first-order, coupled differential equations for the zero- and first-order terms f_0 and f_i , $i = x, y, z$ of the expansion. It has been checked that the energy-distribution function obtained by the first-order truncation provides sufficient accuracy for the problems at hand.^{27,28}

The features of the spherical-harmonics expansion method are illustrated in detail in the above references. To the purposes of this paper it is important to remind the reader that the band structure of the material appears in the model only through the density of states $g(E)$ and group velocity $u_g(E)$ per unit volume in the energy space. The other coefficients of the model are the microscopic relaxation times τ_0 and τ_1 and the electric field \mathbf{F} . The latter is determined from

a simulation using a set of real-space transport equations like those of the hydrodynamic model.²⁹

The density of states and group velocity are obtained directly from the full-band system as³⁰

$$g(E) \doteq \int G(E, \Omega) d\Omega, \quad (1)$$

$$u_g^2(E) \doteq \frac{1}{g(E)} \int G(E, \Omega) U_g^2(E, \Omega) d\Omega, \quad (2)$$

where $G(E, \Omega) = k^3 / (\mathbf{k} \cdot \nabla_{\mathbf{k}} E)$ and $U_g(E, \Omega) = \nabla_{\mathbf{k}} E / \hbar$ are the density of states and group velocity in the \mathbf{k} space, respectively. The carrier concentration, average velocity, and average energy, which are the macroscopic quantities describing the carrier transport, can be calculated from the above. Taking by way of example the electrons of the conduction band, such quantities are given by^{28,29}

$$n = \int g f_0 dE, \quad v_{ni} = \frac{1}{3n} \int u_g f_i dE, \quad w_n = \frac{1}{n} \int E g f_0 dE, \quad (3)$$

where the integrals extend over the conduction band.

The above description shows that the transport coefficients deriving from the material's structure are g and u_g . Therefore, an accurate calculation of the density of states and group velocity is essential for the solution of the carrier-transport problem. The importance of accounting for the full band structure of the material in such a calculation, without resorting to the parabolic-band approximation, has already been outlined in the investigations about carrier transport in silicon.²⁵ As shown by Eqs. (1) and (2), the numerical calculation of g and u_g is based on an integration of the band structure $E(\mathbf{k})$ and its gradient $\nabla_{\mathbf{k}} E(\mathbf{k})$ over the angular part of the \mathbf{k} vector. Thus, an accurate tabulation of the band structure in the \mathbf{k} space is fundamental.

IV. TABULATION OF THE BAND STRUCTURE

The band structures of the SiO_2 polymorphs have been calculated by means of both the HF and DFT methods. The same approach has previously been adopted for the analysis of silicon dioxide, limited to the characteristic directions.⁶ In view of the modeling of the transport phenomena, the generation of numerical tables for the density of states and group velocity is needed. Thus, a three-dimensional mesh in \mathbf{k} space has been generated, and the energy and its derivatives have been calculated at each point. A preliminary part of such work has been the reconstruction of the first Brillouin zone of the polymorphs under investigation from the crystallographic data available in the literature.

Although the calculation at hand could in principle be restricted to the irreducible Brillouin zone, for programming simplicity the band structure has been tabulated over its first octant. This choice does not limit the minimum element size of the adopted mesh: this size is in fact controlled by the CRYSTAL98 code. The critical point of the tabulation procedure is the definition of the geometrical planes of the first Brillouin zones.

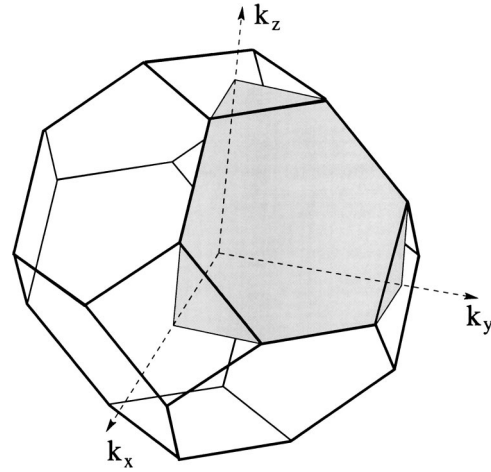


FIG. 1. First Brillouin zone of the β -cristobalite polymorph.

Figure 1 shows the first Brillouin zone of a diamond crystal structure, typical of silicon and β -cristobalite. For this structure, the reciprocal-lattice characteristic vectors are

$$\begin{aligned} \mathbf{b}_1 &= \frac{2\pi}{a} (\mathbf{i}_x + \mathbf{i}_y - \mathbf{i}_z), \\ \mathbf{b}_2 &= \frac{2\pi}{a} (\mathbf{i}_y + \mathbf{i}_z - \mathbf{i}_x), \\ \mathbf{b}_3 &= \frac{2\pi}{a} (\mathbf{i}_x - \mathbf{i}_y + \mathbf{i}_z), \end{aligned} \quad (4)$$

where \mathbf{i}_x , \mathbf{i}_y , and \mathbf{i}_z are orthogonal unit vectors and a is the crystallographic cell parameter of a body-centered cubic structure. The k_x , k_y , and k_z axes of Fig. 1 are parallel to \mathbf{i}_x , \mathbf{i}_y , and \mathbf{i}_z , respectively. In particular, it is $a = 5.42 \text{ \AA}$ for silicon and $a = 7.313 \text{ \AA}$ for β -cristobalite. The first octant, shown in gray in Fig. 1, is defined by the relations

$$0 \leq k_x, k_y, k_z \leq \frac{2\pi}{a}, \quad k_x + k_y + k_z \leq \frac{3}{2} \left(\frac{2\pi}{a} \right). \quad (5)$$

The first equation defines the cube containing the first octant of the Brillouin zone, while the second defines the plane corresponding to the hexagonal face of the figure.

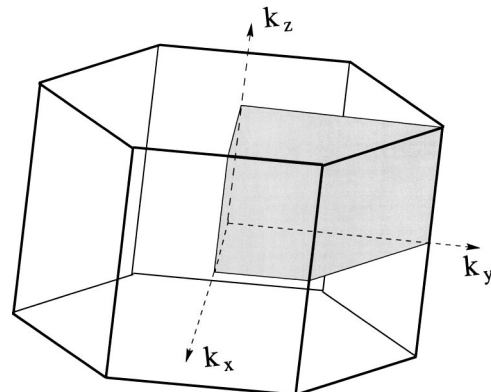
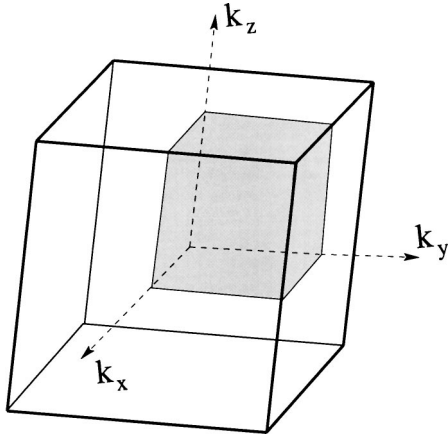


FIG. 2. First Brillouin zone of α - and β -quartz.

FIG. 3. First Brillouin zone of the α -cristobalite polymorph.

The first Brillouin zone of α - and β -quartz is shown in Fig. 2. For these crystals the reciprocal-space characteristic vectors are

$$\begin{aligned} \mathbf{b}_1 &= \frac{2\pi}{a} \mathbf{i}_x, \\ \mathbf{b}_2 &= \frac{2\pi}{a} \left(\frac{1}{2} \mathbf{i}_x + \frac{\sqrt{3}}{2} \mathbf{i}_y \right), \\ \mathbf{b}_3 &= \frac{2\pi}{c} \mathbf{i}_z, \end{aligned} \quad (6)$$

where a and c are the crystallographic parameters of a trigonal structure. In particular, $a = 4.9138 \text{ \AA}$, $c = 5.4052 \text{ \AA}$ for α -quartz, and $a = 4.996 \text{ \AA}$, $c = 5.497 \text{ \AA}$ for β -quartz. In this case, the parallelepiped containing the first octant of the Brillouin zone is defined by

$$\begin{aligned} 0 \leq k_x &\leq \frac{2\pi}{a}, \\ 0 \leq k_y &\leq \frac{2}{\sqrt{3}} \frac{2\pi}{a}, \\ 0 \leq k_z &\leq \frac{2\pi}{c}. \end{aligned} \quad (7)$$

In addition to these relations, the equation of the plane obliquely cutting the (k_x, k_y) plane must be taken into account:

$$k_y \leq -\frac{1}{\sqrt{3}} k_x + \frac{2}{\sqrt{3}} \frac{2\pi}{a}. \quad (8)$$

The relations (7) and (8) together describe the gray region shown in Fig. 2.

Finally, α -cristobalite is characterized by a tetragonal crystal structure, whose first Brillouin zone is shown in Fig. 3. For this kind of crystal the reciprocal-space characteristic vectors are

$$\begin{aligned} \mathbf{b}_1 &= \frac{2\pi}{a} \mathbf{i}_x, \\ \mathbf{b}_2 &= \frac{2\pi}{a} \mathbf{i}_y, \\ \mathbf{b}_3 &= \frac{2\pi}{c} \mathbf{i}_z, \end{aligned} \quad (9)$$

where $a = 4.971 \text{ \AA}$ and $c = 7.010 \text{ \AA}$. The first octant of the Brillouin zone of a tetragonal crystal structure is the parallelepiped defined by the relations

$$\begin{aligned} 0 \leq k_x &\leq \frac{2\pi}{a}, \\ 0 \leq k_y &\leq \frac{2\pi}{a}, \\ 0 \leq k_z &\leq \frac{2\pi}{c}. \end{aligned} \quad (10)$$

For the calculation of the band structure in the first octant of the Brillouin zone, the latter has been discretized. The discretization procedure has been carried out using a $\Delta = 0.05$ mesh step for the k_x , k_y and k_z axes, this defining an elementary, rectangular parallelepiped associated with each discretization point \mathbf{k}_j . More specifically, the distance B_x from the center of the Brillouin zone to the boundary of it, measured along the k_x axis, has been subdivided into equal intervals of length $\Delta_x = B_x \Delta$. The same subdivision has been carried out for the k_y and k_z axes, thus obtaining a set of equal parallelepipeds whose volume depends on the polymorph considered.

In the case of α -cristobalite, due to the shape of the Brillouin zone (Fig. 3), $1/\Delta^3 = 8000$ parallelepipeds fill exactly its first octant, and the number of discretization points turns out to be $(1 + 1/\Delta)^3 = 9261$. In the case of β -cristobalite and α - or β -quartz, the shape of the Brillouin zone prevents an exact filling by parallelepipeds (Figs. 1 and 2). The discretization points turn out to be 5775 for β -cristobalite and 6951 for α - and β -quartz. The choice of the discretization procedure used here stems from the need of interpolating $E(\mathbf{k})$ and $\nabla_{\mathbf{k}} E(\mathbf{k})$. The band structure $E(\mathbf{k})$ is replaced with a quadratic interpolation of the type³¹ over each parallelepiped. Although the quadratic interpolation over parallelepipeds requires the calculation of a larger number of coefficients than the linear one carried out over tetrahedra (see, e.g., Ref. 32), the additional computer load is affordable even when a substantial number of parallelepipeds is used. Moreover, the same type of interpolation is used in Refs. 33 and 34, which makes the comparison sounder (see Sec. VII).

For each discretization point \mathbf{k}_j , the eigenvalues of the eight lowest conduction bands have been computed. Then, the first and second derivatives have been calculated at \mathbf{k}_j as

$$\partial_{\alpha} E_{vj} = \frac{1}{2\Delta_{\alpha}} [E_v(\mathbf{k}_j + \Delta_{\alpha} \mathbf{i}_{\alpha}) - E_v(\mathbf{k}_j - \Delta_{\alpha} \mathbf{i}_{\alpha})], \quad (11)$$

$$\begin{aligned} \partial_{\alpha\beta}^2 E_{vj} = & \frac{1}{4\Delta_\alpha\Delta_\beta} [E_v(\mathbf{k}_j + \Delta_\alpha\mathbf{i}_\alpha + \Delta_\beta\mathbf{i}_\beta) - E_v(\mathbf{k}_j - \Delta_\alpha\mathbf{i}_\alpha \\ & + \Delta_\beta\mathbf{i}_\beta) - E_v(\mathbf{k}_j + \Delta_\alpha\mathbf{i}_\alpha - \Delta_\beta\mathbf{i}_\beta) + E_v(\mathbf{k}_j - \Delta_\alpha\mathbf{i}_\alpha \\ & - \Delta_\beta\mathbf{i}_\beta)], \end{aligned}$$

where v runs over the eight lowest conduction bands, $\Delta_{\alpha(\beta)} = B_{\alpha(\beta)}\Delta$ ($\alpha, \beta = x, y, z$), and $E_{vj} = E_v(\mathbf{k}_j)$.

V. CALCULATION METHOD FOR THE DENSITY OF STATES AND GROUP VELOCITY

In order to determine the density of states g and group velocity u_g at a given energy E , and to finally tabulate them over a wide range of energies, an integration algorithm has been implemented. A brief description is given in the following, with special emphasis for the numerical aspects. Using the coordinates of the \mathbf{k} space, Eqs. (1) and (2) read

$$g(E) = \frac{2}{(2\pi)^3} \sum_v \int_k \delta(E - E_v(\mathbf{k})) d\mathbf{k}, \quad (12)$$

$$u_g^2(E)g(E) = \frac{2}{(2\pi)^3} \sum_v \int_k u_v^2(\mathbf{k}) \delta(E - E_v(\mathbf{k})) d\mathbf{k}, \quad (13)$$

where $1/(2\pi)^3$ is the density of states in the (\mathbf{r}, \mathbf{k}) space, v is the band index, $u_v = (1/\hbar)\nabla_k E_v$, and the factor 2 accounts for the spin degeneracy.

The energy range 0–10 eV has been chosen for the application of the algorithm, in order to cover the eight lowest conduction bands for all the polymorphs of interest. Such a range has been divided into 500 equal intervals of 0.02 eV each.

The integrals (12) and (13) must be carried out over surfaces of constant energy $E = E_v(\mathbf{k})$, where $E_v(\mathbf{k})$ is given by a table in which \mathbf{k} is discretized as detailed in the preceding section. The algorithm runs over the elementary parallelepipeds introduced in Sec. IV. The vertices of the m th parallelepiped will be denoted here as \mathbf{k}_{mi} , $i = 1, \dots, 8$ where, in particular, \mathbf{k}_{m1} corresponds to the vertex where the sum $k_x + k_y + k_z$ is minimum. If the current energy level E is in the range defined by the eigenvalues $E_v(\mathbf{k}_{mi})$, then the m th parallelepiped contributes to the calculation of the number of states.

Following Ref. 31, the number of states per eV and unit volume of the m th parallelepiped and v th band can be approximated as

$$S_{vm} = \frac{A_{vm}}{|\nabla_k E_v(\mathbf{k}_{mc})|}, \quad (14)$$

where A_{vm} is the surface determined by the intersection of the isoenergetic plane with the parallelepiped. Equation (14) replaces the actual energy surface to which the center \mathbf{k}_{mc} of the m th parallelepiped belongs with a plane normal to $\nabla_k E_v(\mathbf{k}_{mc})$. As a consequence, to implement Eq. (14) it is necessary to interpolate $E_v(\mathbf{k}_{mc})$ and the corresponding gra-

dient. Summation over the parallelepipeds and bands gives the final density of states corresponding to the current level E .

The interpolation has been implemented here as follows: first, the parallelepiped center \mathbf{k}_{mc} is calculated and, for a given band v , the corresponding energy is determined as a first approximation from a quadratic interpolation starting from the parallelepiped's vertices:

$$\begin{aligned} E_{vi}(\mathbf{k}_{mc}) = & E_{vi}(\mathbf{k}_i) + \sum_\alpha \partial_\alpha E_{vi}(\mathbf{k}_i)(k_{\alpha mc} - k_{\alpha mi}) \\ & + \frac{1}{2} \sum_{\alpha\beta} \partial_{\alpha\beta}^2 E_{vi}(\mathbf{k}_i)(k_{\alpha mc} - k_{\alpha mi})(k_{\beta mc} - k_{\beta mi}). \end{aligned} \quad (15)$$

Consistently, the component of the group velocity in the \mathbf{i}_α direction is approximated as

$$\begin{aligned} u_{vi\alpha}(\mathbf{k}_{mc}) = & \frac{1}{\hbar} \nabla_k E_{vi} \cdot \mathbf{i}_\alpha = \partial_\alpha E_{vi}(\mathbf{k}_i) \\ & + \sum_\beta \partial_{\alpha\beta}^2 E_{vi}(\mathbf{k}_i)(k_{\beta mc} - k_{\beta mi}). \end{aligned} \quad (16)$$

Then, the approximation is improved by averaging over the vertices: $E_v(\mathbf{k}_{mc}) = \sum_{i=1}^8 E_{vi}(\mathbf{k}_{mc})/8$, and the same for $u_{vi\alpha}(\mathbf{k}_{mc})$.

The group velocity as a function of E is obtained in a similar way. It is worth noting that an alternative definition of the group velocity is³⁴

$$u_g(E)g(E) = \frac{2}{(2\pi)^3} \sum_v \int_k |\mathbf{u}_v(\mathbf{k})| \delta(E - E_v(\mathbf{k})) d\mathbf{k}. \quad (17)$$

The computation shows that for the materials at hand the difference between the group velocity derived from Eq. (13) and that of Eq. (17) is not quantitatively relevant. An example is shown in Fig. 5.

VI. OPTIMIZATION OF THE BASIS SETS

A first critical aspect of the numerical calculation of the band structure in SiO₂ has been the choice of the variational basis set to accurately describe the atomic orbitals. The variational basis sets adopted in this work for the SiO₂ polymorphs have been obtained starting from a number of optimized sets for α -quartz reported in Ref. 35. First, as the Si—O bond is quite ionic, the choice of the basis is more critical for oxygen than for silicon. For this reason, a 6-211G(2d) basis instead of a 6-21G(2d) has been chosen for oxygen.³⁵ A slightly different basis set has been adopted for β -quartz in order to overcome some convergence problems. The symbols used to indicate the basis sets are standard.⁴²

Since the choice of the basis set plays an essential role in the description of the electronic structure and in the calculation of the conduction-band eigenvalues, the basis sets for β -quartz, α -cristobalite, and β -cristobalite have been opti-

TABLE I. Adopted basis sets for silicon and oxygen.

Atoms	Basis set	Gaussian exponents
<i>α-quartz</i>		
Si	6-21G(2 <i>d</i>)	$\alpha_{sp}=0.130$ $\alpha_{d1}=0.500$ $\alpha_{d2}=1.500$
O	6-211G(2 <i>d</i>)	$\alpha_{sp1}=0.890$ $\alpha_{sp2}=0.280$ $\alpha_{d1}=0.400$ $\alpha_{d2}=1.200$
<i>β-quartz</i>		
Si	6-21G(2 <i>d</i>)	$\alpha_{sp}=0.130$ $\alpha_d=0.500$
O	6-31G(2 <i>d</i>)	$\alpha_{sp}=0.274$ $\alpha_d=0.600$
<i>α-cristobalite</i>		
Si	6-21G(2 <i>d</i>)	$\alpha_{sp}=0.119$ $\alpha_{d1}=0.429$ $\alpha_{d2}=1.289$
O	6-211G(2 <i>d</i>)	$\alpha_{sp1}=1.317$ $\alpha_{sp2}=0.414$ $\alpha_{d1}=0.242$ $\alpha_{d2}=0.728$
<i>β-cristobalite</i>		
Si	6-21G(2 <i>d</i>)	$\alpha_{sp}=0.113$ $\alpha_{d1}=0.856$ $\alpha_{d2}=2.568$
O	6-211G(2 <i>d</i>)	$\alpha_{sp1}=1.309$ $\alpha_{sp2}=0.411$ $\alpha_{d1}=0.200$ $\alpha_{d2}=0.602$

mized as well. Starting from the values reported in Ref. 35, a nonlinear parameter optimization has been carried out. The optimization procedure is based on the nonlinear modified damped least-square scheme, an improved variant of the Levenberg-Marquardt method^{36,37} and, in the present case, has led to optimizing the basis-set parameters with respect to a final fitting value for the minimum energy. Only the exponents for the Gaussian functions describing the outer orbitals for the silicon and oxygen atoms have been exploited for this optimization. The nonlinear optimization has been carried out with four parameters in order to limit the computational load. Such parameters are the scaling factors affecting the exponents of the Gaussian functions.

It is worth mentioning that, as in the variational HF method the calculated energy is always above the experimental one, a decrease in energy corresponds to an improved basis set. For this reason, the parameter optimization has been carried out in the frame of the HF approach. Once the optimal parameters have been determined, the corresponding basis set has been adopted also for the DFT calculation.

In Table I, the adopted basis sets for the polymorphs un-

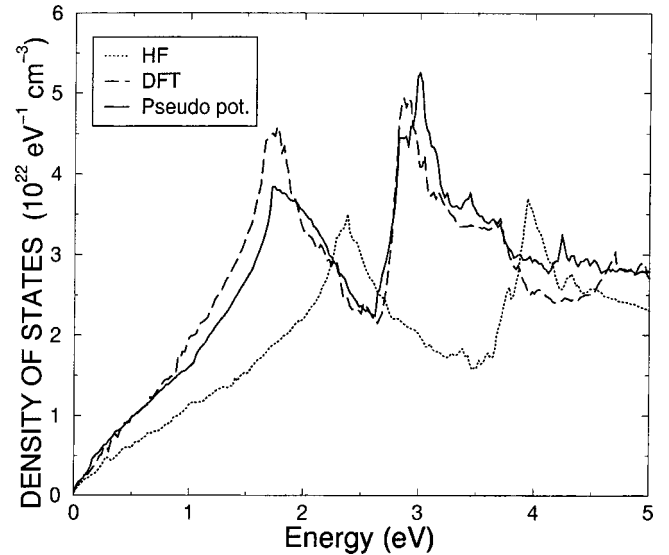


FIG. 4. Density of states in energy for silicon. Solid line: pseudopotentials (Ref. 34). Dotted line: HF method. Dashed line: DFT method.

der study and the exponents for the Gaussian functions describing the outer orbitals for the silicon and oxygen atoms are reported, rounded to four digits. Starting from the α -quartz basis set of Ref. 35, the first scaling factor refers to the sp shells, the second factor refers to the d shells of the silicon atom, the third and fourth factors refer to the sp and d shells of the oxygen atom, respectively.

VII. RESULTS AND CONCLUSIONS

The results of band calculations obtained by the procedure depicted above have been exploited to calculate the density-of-state and group-velocity functions as described in Secs. IV and V. The numerical accuracy in the description of such functions demanded by the SHE method is very high. Special care has then been devoted to the definition of the three-dimensional mesh in the \mathbf{k} space and to the algorithm for calculating the two functions.

A first test has been carried out to validate the method: both the density of states and group velocity have been calculated for Si and compared to those given by Ref. 34. The density of states computed by the DET band structure is compared in Fig. 4 with that given by the pseudopotential approach of Ref. 34. In the latter reference, the band structure is obtained following the local empirical pseudopotential method by Cohen and Bergstresser³⁸ after adjusting the form factors to the material under investigation.

Both the qualitative shape of the function and the value and position of the main peaks are very similar for the two techniques. The maximum relative difference between the two sets is about 15%. Despite the differences between the DFT and HF methods, the calculated energy bands are usually similar to each other. The DFT eigenvalues are in general slightly lower than the HF ones, and the energy-band gap is usually underestimated with respect to the experiments. As far as the calculation of the density of states by the

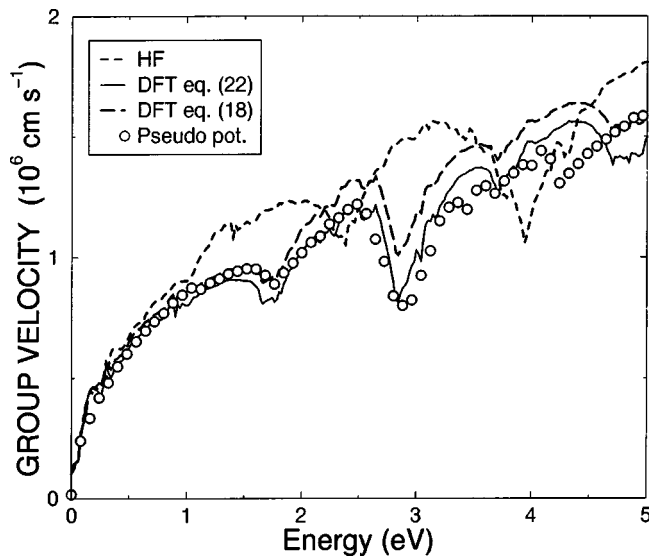


FIG. 5. Group velocity in energy for silicon. Dots: pseudopotentials (Ref. 34). Dashed line: HF method. Solid line: DFT method using definition (17). Long-dashed line: DFT method using definition (13).

HF method is concerned, even if a qualitative agreement can be recognized, a rather different distribution in the number of states is found in the whole range of energies: this discrepancy is intrinsic to the method and is due to the overestimation of the eigenvalues given by the HF approach, this suggesting that the HF technique is less suited to this kind of analysis. In Fig. 5, the results of the group-velocity calculation for silicon have been reported and compared with the

data of Ref. 34. The results provided by the DFT approach are again very similar to those of Ref. 34. The comparison of Fig. 4 shows that the DFT method reproduces well the density of states of the conduction band. The same agreement between the pseudopotential and DFT methods can be seen in Fig. 5 for the group velocity [even when two alternative definitions of the latter are adopted, Eqs. (13) and (17)]. In addition, DFT agrees with the pseudopotential results better than the HF method.

After completing the validation of the algorithms adopted for the calculation of the electronic properties, the procedure has been applied to the full band structures of the polymorphs under study. In Fig. 6, the densities of states for the four structures are shown. Both the DFT and HF data have been reported: here again, the overestimation of the HF eigenstates gives a clear shift of the main peaks to higher energies. As far as the comparison between the polymorphs is concerned, a strong similarity is found between the shapes of the density of states in the whole range. The agreement is also quantitative for energies up to 3 eV. Similar features are visible in the group velocities. The latter are shown in Fig. 7, where the velocities obtained with both HF and DFT methods are reported.

To summarize, the investigations described so far led to the following results: (i) implementation of a tabulation algorithm for the energy bands in the first Brillouin zone of the materials of interest, including the preliminary reconstruction of the Brillouin zone from the crystal logographic data available in the literature, (ii) calculation of the first eight conduction bands—covering the energy range of interest—for a number of silica polymorphs, including the optimization of

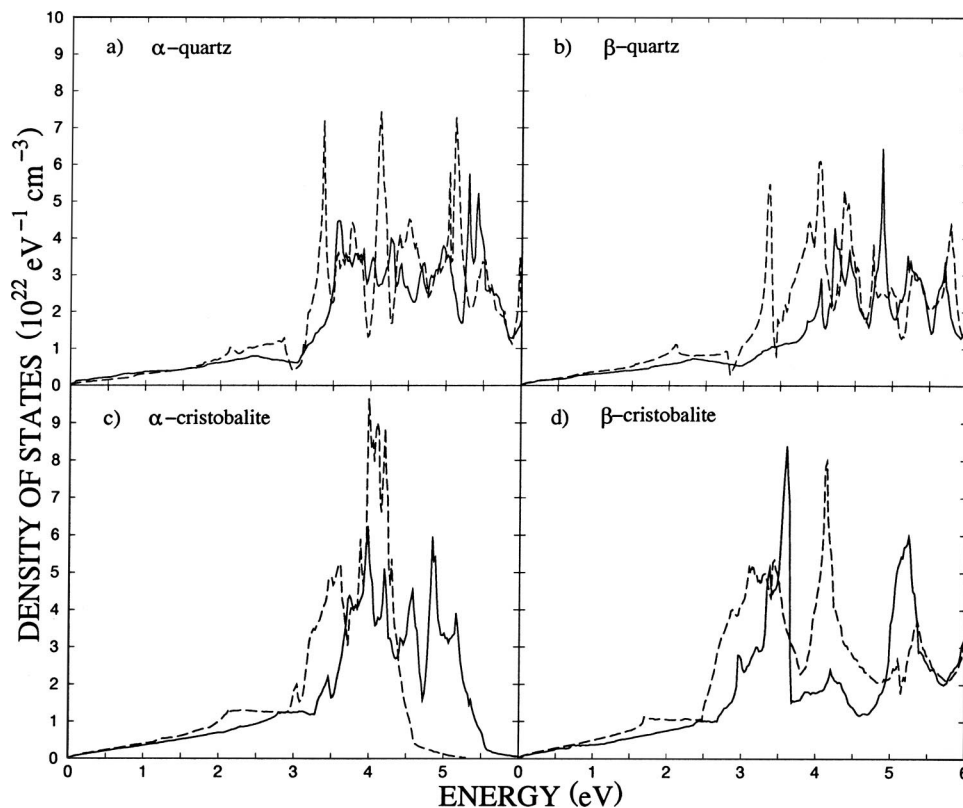


FIG. 6. Density of states in energy for (a) α -quartz, (b) β -quartz, (c) α -cristobalite, and (d) β -cristobalite. Solid lines: HF method. Dashed lines: DFT method.

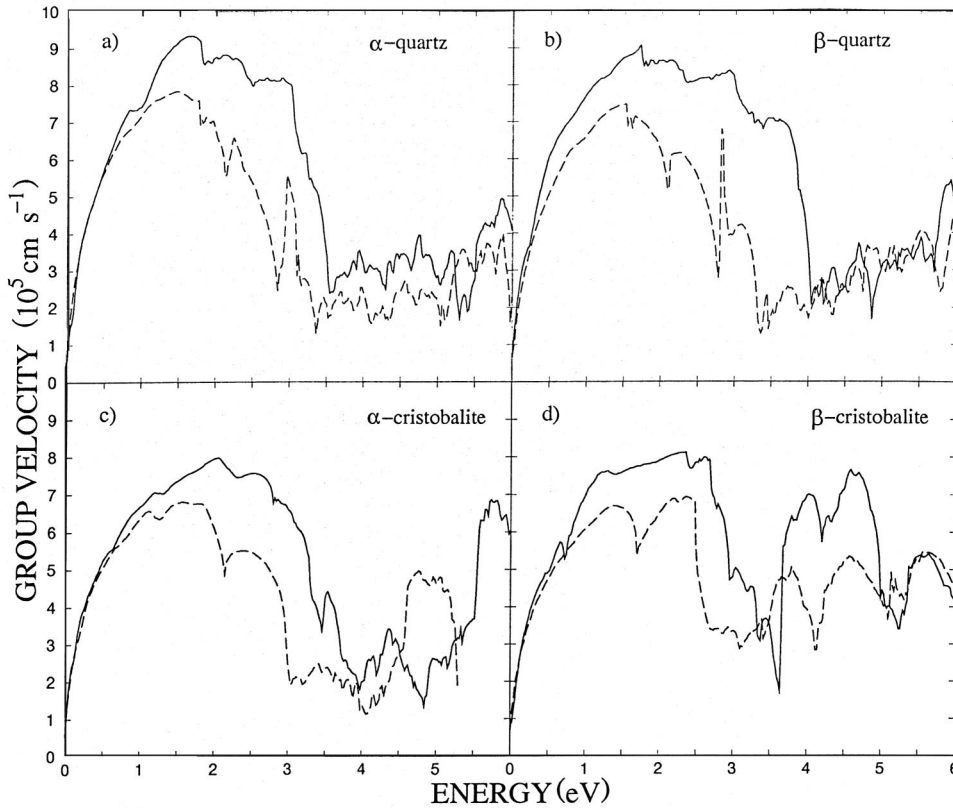


FIG. 7. Group velocity in energy for (a) α -quartz, (b) β -quartz, (c) α -cristobalite, and (d) β -cristobalite. Solid lines: HF method. Dashed lines: DFT method.

the basis set for both silicon and oxygen, (iii) implementation of a systematic interpolation scheme for the calculation of the density of states and group velocity, based on Eq. (14), starting from the tabulation of the eigenvalues, and (iv) application of the interpolation scheme to the silica polymorphs and to silicon, including the comparison of the two possible definitions (13) and (17) of the group velocity.

As mentioned above, the density of states and group velocity of silicon were already known, and their calculation has been carried out here in order to validate our procedure by comparison with a consistent set of data available in Ref. 34. As far as the group velocities of silica polymorphs are concerned, no data are available, at least to the authors' knowledge. The results shown here are thus a contribution to the self-consistent calculation of a complete set of coefficients of the Boltzmann transport equation within the SiO_2 domain, in the framework of the solution method based on the spherical-harmonics expansion.

Extending the approach of Ref. 1, the individual scattering rates of collision processes relevant in bulk SiO_2 have been modeled accounting for the full band structure. The processes are related to two modes of the polar longitudinal-optical phonons (LO), to the transverse-optical phonons (TO), and to the acoustic phonons (AC). They contribute to the total scattering rate $1/\tau_0$ according to

$$\frac{1}{\tau_0} = c_{\text{LOG}}^{(1)}(E \mp \hbar \omega_{\text{LO}}^{(1)}) + c_{\text{LOG}}^{(2)}(E \mp \hbar \omega_{\text{LO}}^{(2)}) + c_{\text{TOG}}(E \mp \hbar \omega_{\text{TO}}) + c_{\text{ACG}}(E). \quad (18)$$

The definition of $c_{\text{LO}}^{(1)}$, $c_{\text{LO}}^{(2)}$, c_{TO} , c_{AC} is given in Ref. 1, along with that of the other relaxation time τ_1 in terms of the same scattering processes as τ_0 . Each coefficient of Eq. (18) embeds a multiplicative constant whose value has been determined by comparison with the experimental data as outlined below.

By way of example, the zero- and first-order terms of the distribution function's expansion f_0 , and f_i have been determined by solving the Boltzmann transport equation in the spatially uniform case, with a constant electric field $\mathbf{F} = F\mathbf{i}_x$ and using the density of states and group velocity of β -cristobalite calculated with the DFT technique. The electron concentration, average velocity, and average energy have then been calculated from Eq. (3). In this case the electron mobility is given by the drift relation $v_{nx} = \mu_n F$, where v_{nx} is derived by setting $f_i = f_x$ in Eq. (3).

The results are shown in Figs. 8 and 9. In the first one, the calculated mobility is compared with the experimental results of Ref. 39, which have been obtained from SiO_2 samples of different thicknesses. In the second, the calculated average energy is compared with the same quantity determined from the parabolic-band approximation, and with experimental results of Refs. 3 and 40 obtained with the carrier-separation technique. It is worth mentioning that the experimental setup for measuring energy using such a technique is known to provide more reliable results at higher fields.⁴¹ For this reason, the data below 5 MV/cm have not been used in the fitting procedure. It can also be observed that in the mobility data of Fig. 8 the sets corresponding to different thicknesses exhibit a nonmonotonic dependence on

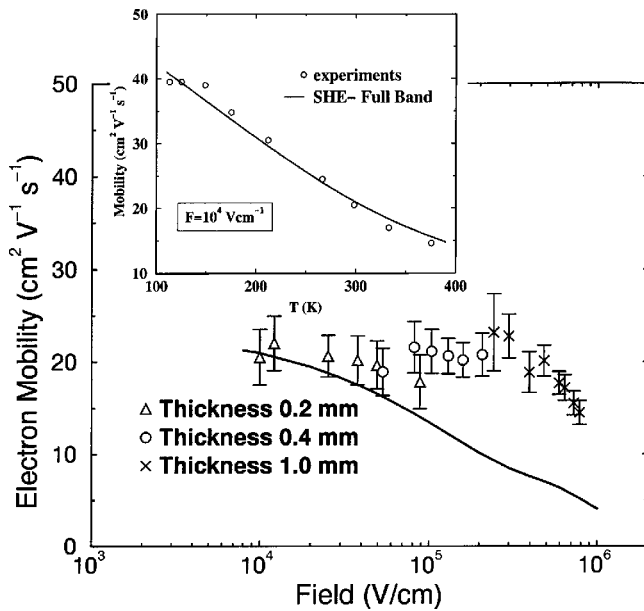


FIG. 8. Electron mobility in SiO_2 as a function of the electric field. Symbols show the experimental results reported in Ref. 39, obtained on samples with different thicknesses. The inset compares the calculated mobility with that measured by Ref. 39 on the lowest-thickness sample, as a function of temperature and with $F = 10^4$ V/cm.

the field, which makes the fitting based on these sets less appropriate. On the other hand, a sound fitting procedure should take the mobility and average-energy data into account at the same time, because they are related to different moments of the distribution function. Another set of data is available in Ref. 39, which reports the electron mobility for the lowest-thickness sample as a function of temperature at $F = 10^4$ V/cm. This set of data is better suited for the fitting procedure due to the strong temperature dependence of the phonon scattering and, in addition, because it makes the fitting domain two-dimensional as temperature and electric field are independent.

In conclusion, the multiplicative constants within the coefficients of Eq. (18) have been determined by a simultaneous fitting of the mobility data as a function of temperature and of the average-energy data as a function of the electric field. The inset of Fig. 8 compares the calculated and experimental mobility as a function of temperature in the range 100–400 K. After completing the fitting, the electron mobility as a function of the electric field has been calculated with

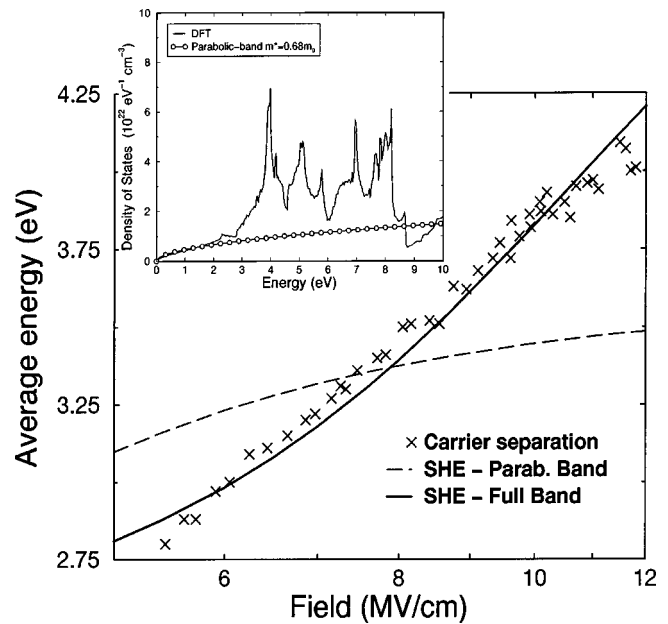


FIG. 9. Electron average energy in SiO_2 as a function of the electric field, calculated by the spherical-harmonics method (SHE) using the parabolic-band (dashed line) and full-band structure (continuous line). The symbols show the experimental results reported in Refs. 3 and 40. The inset compares the full-band density of states of β -cristobalite with that obtained from the parabolic-band model.

no further change in the multiplicative constants of Eq. (18), to obtain the results shown in Fig. 8. As expected, the agreement is better for the lowest-thickness sample. As for the average energy (Fig. 9), the agreement is fair in the high-field range. A final observation is about the relevance of the full band calculation. The dashed curve in Fig. 9 shows the result of the same fitting procedure as above carried out using the parabolic-band model. The marked saturation behavior is due to the much lower number of electronic states at higher energies. The difference in the densities of states for microscopic energies larger than 2 eV can be appreciated in the curves shown in the inset, where the full band and parabolic-band cases are compared.

The investigation reported in this work is part of a larger project aimed at solving the carrier transport in semiconductor devices, in the framework of the semiclassical Boltzmann transport equation in real space and energy. Such information, coupled with that already available for silicon, builds up the physical basis for the full band calculation of the distribution function in the whole MOS structure.

¹L. Scozzoli, S. Reggiani, and M. Rudan, *IEICE Trans. Electron.* (Special Issue on SISPAD99) **E83-C**, 1183 (2000).

²M. Marsella, S. Reggiani, A. Gnudi, and M. Rudan, in *Proceedings of the 30th European Solid-State Device Research Conference (ESSDERC), Ireland, 2000*, edited by W. A. Lane, G. M. Crean, F. A. McCabe, and H. Grunbacher (Edition Frontiers, Cork, Ireland, 2000), p. 604.

³M. V. Fischetti, *Phys. Rev. Lett.* **53**, 1755 (1984).

⁴W. Porod and D. K. Ferry, *Phys. Rev. Lett.* **54**, 1189 (1985).

⁵D. Arnold, E. Cartier, and D. J. DiMaria, *Phys. Rev. B* **49**, 10 278 (1994).

⁶E. Gnani, S. Reggiani, R. Colle, and M. Rudan, *IEEE Trans. Electron Devices* **47**, 1795 (2000).

⁷A. D. Becke, *J. Chem. Phys.* **98**, 5648 (1993).

- ⁸C. Lee, W. Yang, and R. G. Parr, Phys. Rev. B **37**, 785 (1988).
- ⁹P. M. Schneider and W. B. Fowler, Phys. Rev. Lett. **36**, 425 (1976).
- ¹⁰J. R. Chelikowsky and M. Schlüter, Phys. Rev. B **15**, 4020 (1977).
- ¹¹P. M. Schneider and W. B. Fowler, Phys. Rev. B **18**, 7122 (1978).
- ¹²E. Calabrese and W. B. Fowler, Phys. Rev. B **18**, 2888 (1978).
- ¹³Y. Xu and W. Y. Ching, Phys. Rev. B **44**, 11 048 (1991).
- ¹⁴C. Persson and U. Lindefelt, J. Appl. Phys. **83**, 266 (1998).
- ¹⁵P. K. Chakraborty and J. C. Biswas, J. Appl. Phys. **82**, 3328 (1997).
- ¹⁶O. K. B. Lui, S. W. B. Tam, P. Migliorato, and T. Shimoda, J. Appl. Phys. **89**, 6453 (2001).
- ¹⁷M. Städele, B. R. Tuttle, and K. Hess, J. Appl. Phys. **89**, 348 (2001).
- ¹⁸A. A. Demkov, X. Zhang, and D. A. Drabold, Phys. Rev. B **64**, 125306 (2001).
- ¹⁹K. Hübner, Phys. Status Solidi A **40**, 487 (1977).
- ²⁰H. R. Philipp, J. Phys. Chem. Solids **32**, 1935 (1971).
- ²¹A. D. Pomponio, A. Continenza, L. Lozzi, M. Passacantando, S. Santucci, and P. Picozzi, Solid State Commun. **95**, 313 (1995).
- ²²R. Dovesi, C. Roetti, M. Causà, V. R. Saunders, and N. M. Harrison, *Crystal98—User's Manual* (Theoretical Chemistry Group, University of Torino and Computational Materials Science Group, CRLC Daresbury Laboratory, 1999).
- ²³D. Ventura, A. Gnudi, and G. Baccarani, Riv. Nuovo Cimento **18**, 1 (1995).
- ²⁴D. Ventura, A. Gnudi, and G. Baccarani, Appl. Math. Lett. **5**, 85 (1992).
- ²⁵M. C. Vecchi and M. Rudan, IEEE Trans. Electron Devices **45**, 230 (1998).
- ²⁶A. Gnudi, D. Ventura, G. Baccarani, and F. Odeh, Solid-State Electron. **36**, 575 (1993).
- ²⁷M. C. Vecchi, D. Ventura, A. Gnudi, and G. Baccarani, in *Proceedings of the NUPAD V Conference*, edited by H. S. Bennett and M. E. Law (IEEE, Honolulu, 1994), pp. 55–58.
- ²⁸D. Ventura, A. Gnudi, and G. Baccarani, IEICE Trans. Electron. **75-C**, 194 (1992).
- ²⁹S. Taschini, M. Rudan, and R. Brunetti, Phys. Rev. B **60**, 13 582 (1999).
- ³⁰M. V. Fischetti and S. E. Laux, Phys. Rev. B **38**, 9721 (1988).
- ³¹G. Gilat and L. J. Raubenheimer, Comput. Phys. Commun. **20**, 349 (1980).
- ³²G. Lehmann and M. Taut, Phys. Status Solidi B **54**, 469 (1972).
- ³³S. E. Laux, M. V. Fischetti, and D. J. Franck, IBM J. Res. Dev. **34**, 1663 (1990).
- ³⁴M. V. Fischetti, IEEE Trans. Electron Devices **38**, 634 (1991).
- ³⁵B. Civalieri, P. Ugliengo, and R. Dovesi, Chem. Phys. Lett. **292**, 394 (1998).
- ³⁶G. L. Ouwering, Profile User's Manual, (Delft University of Technology, Delft, 1987).
- ³⁷G. J. L. Ouwering, F. van Rijs, B. F. P. Jansen, and W. Crans, in *Short Course on Software Tools for Process, Device and Circuit Modelling*, of the Digest of the NASECODE VI Software Forum, edited by W. Crans (Boole Press, Dublin, 1989), pp. 78–89.
- ³⁸M. L. Cohen and T. K. Bergstresser, Phys. Rev. **141**, 789 (1966).
- ³⁹R. Hughes, Phys. Rev. Lett. **30**, 1333 (1973).
- ⁴⁰M. V. Fischetti and D. J. DiMaria, Solid-State Electron. **31**, 629 (1988).
- ⁴¹D. J. Maria, T. N. Theis, J. R. Kirtley, F. L. Pesavento, D. W. Dong, and S. D. Brorson, J. Appl. Phys. **57**, 1214 (1985).
- ⁴²With reference to Table I, the 6-21G(2d) code defines a function set given by six Pople standard [D. J. Hehre, L. Radom, and J. A. Pople, *Ab Initio Molecular Orbital Theory* (Wiley, New York, 1986)]. Gaussian functions for the $1s_2$ orbital, six Pople standard functions for the $2s_2$ and $2p_6$ orbitals, and two Pople standard function for the $3s_2$ and $3p_2$ orbitals. As far as the outer orbitals are concerned, one sp function and two d shells have been added to accurately describe the electronic structure of silicon. Similarly, a 6-211G(2d) basis set has been adopted for the oxygen atom, given by six Pople standard functions for the $1s_2$ orbital, two Pople standard functions for the $2s_2$ and $2p_4$ orbitals and, in addition, two more sp and d shells.